

X-RAY SURFACE BRIGHTNESS PROFILES OF ACTIVE GALACTIC NUCLEI IN THE EXTENDED GROTH STRIP: IMPLICATIONS FOR AGN FEEDBACK

SUCHETANA CHATTERJEE^{1,2,3}, JEFFREY A. NEWMAN^{1,4}, TESLA JELTEMA⁵, ADAM D. MYERS², JAMES AIRD⁶, ALISON L. COIL⁷,
MICHAEL COOPER⁸, ALEXIS FINO GUENOV^{9,10}, ELISE LAIRD¹¹, ANTONIO MONTERO-DORTA¹², KIRPAL NANDRA¹³, CHRISTOPHER
WILLMER¹⁴, RENBIN YAN¹⁵

¹Department of Physics and Astronomy, University of Pittsburgh, Pittsburgh, PA 15260, USA

²Department of Physics and Astronomy, University of Wyoming, Laramie, WY 82072, USA

³Yale Center for Astronomy and Astrophysics, Department of Physics, Yale University, New Haven, CT 06520, USA

⁴PITT-PACC, University of Pittsburgh, Pittsburgh, PA 15260, USA

⁵Department of Physics, University of California, Santa Cruz, CA 95064, USA

⁶Department of Physics, Durham University, Durham DH13LE, UK

⁷Department of Physics, University of California, San Diego, CA 92093, USA

⁸Department of Physics and Astronomy, University of California, Irvine, CA 92697, USA

⁹Department of Physics, University of Helsinki, Helsinki, Finland

¹⁰Center for Space Science Technology, University of Maryland Baltimore County, Baltimore, MD 21250, USA

¹¹Astrophysics Group, Imperial College London, Blackett Laboratory, Prince Consort Road, London SW7 2AZ, UK

¹²Department of Physics and Astronomy, University of Utah, Salt Lake City, UT 84112, USA

¹³Max Planck Institut für Extraterrestrische Physik, Giessenbachstraße, 85748 Garching, Germany

¹⁴Steward Observatory, University of Arizona, Tucson, AZ, 85721, USA

¹⁵Department of Physics and Astronomy, University of Kentucky, Lexington, KY 40506, USA

Draft version July 5, 2019

ABSTRACT

Using data from the All Wavelength Extended Groth Strip International Survey (AEGIS) we statistically detect the extended X-ray emission in the interstellar medium (ISM) in both active and normal galaxies at $0.3 \leq z \leq 1.3$. For both active galactic nuclei (AGN) host galaxy and normal galaxy samples that are matched in restframe color, luminosity, and redshift distribution, we detect excess X-ray emission at scales of 40–60 kpc at 1–4 σ significance. We study the effect of feedback from AGN on the diffuse ISM gas by comparing the stacked X-ray surface brightness profiles of active and normal galaxies. In accordance with theoretical studies we detect a slight deficit ($< 1.5\sigma$) of X-ray photons when averaged over a scale of 0–30 kpc in the profile of AGN host galaxies at $0.3 \leq z \leq 0.7$. The equivalent flux deficit is $(1.25 \pm 0.75) \times 10^{-19}$ ergs s⁻¹ cm⁻². When averaged over a scale of 30–60 kpc, beyond the PSF scales of our AGN sources, we observe a $\sim 2\sigma$ photon excess in the profile of the AGN host galaxies with an equivalent flux excess of $(1.1 \pm 0.5) \times 10^{-19}$ ergs s⁻¹ cm⁻². Such deficits and excess in flux at similar scales have been theoretically predicted and could be a potential signature of AGN-ISM interaction. We propose that AGN that are intrinsically under luminous in X-rays, but have equivalent bolometric luminosities to our sources will be the ideal sample to study more robustly the effect of AGN feedback on the diffuse ISM gas.

Subject headings: galaxies: active, galaxies:ISM, ICM, AGN:general, Xrays:ISM, galaxies

1. INTRODUCTION

Several lines of evidence suggest that energy input from active galactic nuclei (commonly known as AGN feedback) can have substantial effects on the formation and evolution of galaxies. For example, the observed correlation between black hole mass-bulge mass (e.g., Gebhardt et al. 2000; Merritt & Ferrarese 2001; Tremaine et al. 2002) strongly implies a connection between galaxy formation and black hole growth. The observed lack of expected cooling flows in galaxy clusters and the exponential cut-off at the bright end of the galaxy luminosity function have been also linked with AGN feedback (e.g., Peterson & Fabian 2006; Croton et al. 2006).

Effects of AGN feedback have been directly observed in groups and clusters using multi-wavelength data. For example, AGN residing in cluster centers have supermassive black holes, which accrete matter from the intra-cluster medium (ICM), releasing tremendous amounts of energy in radiation and/or outflows. This has been observed with X-rays in cluster cores (e.g., McNamara & Nulsen 2007). With the

emergence of *Chandra* and XMM-Newton, the evidence that the central radio sources in groups and clusters have a profound, persistent effect on the ICM has been strongly established. It has been shown that the deficits in the X-ray emission in clusters (X-ray cavities) are spatially coincident with regions of high synchrotron emission (e.g., Birzan et al. 2004; Nulsen et al. 2005; Dunn & Fabian 2006; McNamara & Nulsen 2007; Gitti et al. 2012). Galaxy groups have shallower potential wells and hence smaller intrinsic thermal energy. Thus AGN outbursts have a large impact on the intragroup medium (e.g., Giodini et al. 2010). Investigating X-ray cavities and their connection with AGN activity in the intragroup medium have been undertaken in different studies (e.g., Johnson et al. 2009; O’Sullivan et al. 2010; Dong et al. 2010; Randall et al. 2011).

Several theoretical models relating AGN activity to galaxy evolution have been proposed in this context. In many of these models AGN feedback is introduced in the form of thermal energy feedback which naturally explains the $M - \sigma$ relation and exponential cut-off of the bright end of the

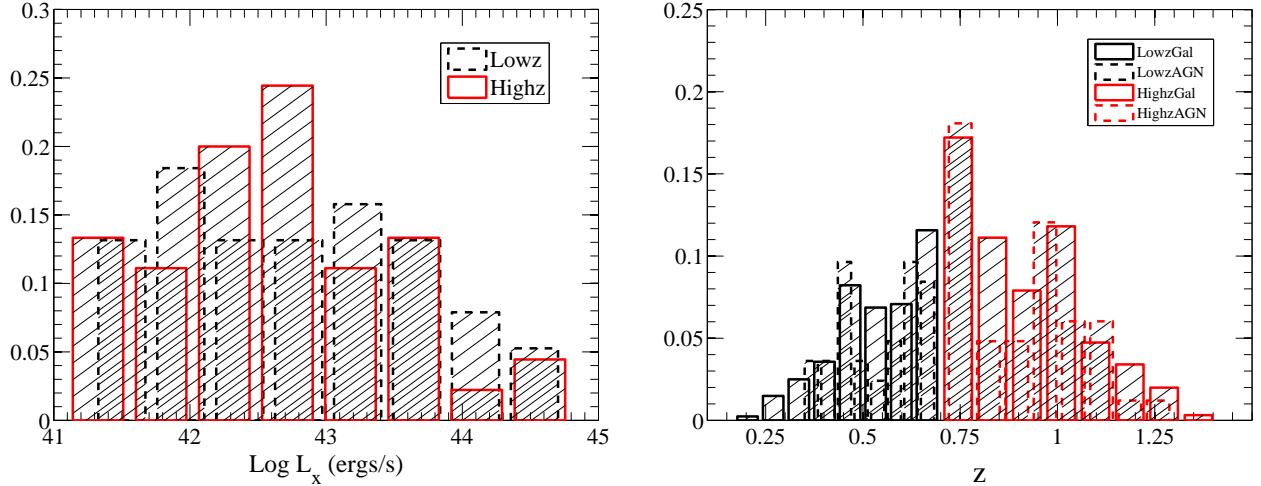


FIG. 1.— Distribution of soft X-ray luminosity (left panel) and redshift (right panel) of our X-ray AGN sources (L09 sample). We present the luminosity and redshift distributions of our two subsamples, namely the *Lowz* ($0.3 \leq z \leq 0.7$) and *Highz* ($0.7 \leq z \leq 1.3$) samples, which we construct from the parent sample for our analysis. In the left panel the red solid and the black dashed histograms show the distribution of X-ray luminosities for the *Highz* and *Lowz* samples respectively. The solid and the dashed histograms in the right panel represent the redshift distributions of the galaxy control samples and the AGN samples respectively. Red and black refer to the *Highz* and *Lowz* samples. The distributions in both the panels are normalized by the total number of objects in each subsample. See §2 for more details. The binsizes and labels are slightly different for each sample which explains the shift in the histograms.

galaxy luminosity function (e.g., Kauffmann & Haehnelt 2000; Ciotti & Ostriker 2001; Wyithe & Loeb 2003; Marconi et al. 2004; Shankar et al. 2004; Di Matteo et al. 2005; Cattaneo et al. 2006; Croton et al. 2006; Hopkins et al. 2006; Lapi et al. 2006; Booth & Schaye 2009; Teyssier et al. 2011; Johansson et al. 2008). Some models do include momentum feedback (e.g., Sijacki et al. 2007; Ciotti & Ostriker 2007; Novak et al. 2011; Gaspari et al. 2011, 2012; Choi et al. 2012, 2013) but the scales and physical processes vary widely between them.

The effect of feedback on several observables has been explored in the literature, including the $L_x - T$ relation in galaxy clusters and groups (e.g. Arnaud & Evrard 1999; Nath & Roychowdhury 2002; Scannapieco & Oh 2004; Peterson & Fabian 2006; Thacker et al. 2009; Puchwein et al. 2010), Sunyaev-Zeldovich (SZ; Sunyaev & Zeldovich 1972) profiles (e.g., Bhattacharya et al. 2008; Chatterjee et al. 2008, 2010), SZ power spectrum (e.g., Chatterjee & Kosowsky 2007; Scannapieco et al. 2008; Battaglia et al. 2010), and star-formation properties of galaxies (e.g., Di Matteo et al. 2005; Cattaneo et al. 2006; Croton et al. 2006; Hopkins et al. 2006; Schawinski et al. 2007).

Recently, Pellegrini et al. (2012, P12 hereafter) performed a one-dimensional hydrodynamic simulation using a physically motivated prescription for AGN feedback in elliptical galaxies to explore its effect on the X-ray properties of the interstellar medium (ISM). The simulation predicts a decrease of flux in the surface brightness profiles near the central region of the galaxy compared to models without AGN feedback. The model also predicts a change in the slope and normalization of the soft X-ray surface brightness profile which extends to a scale of 50 – 100 kpc. Motivated in part by the predictions of P12 we now investigate the impact of AGN on their large-scale environments by examining the properties of the diffuse X-ray emitting gas in AGN host galaxies at high redshifts ($z \sim 0.8$).

By using a large sample of active and normal galaxies

which have identical optical properties we statistically compare their diffuse X-ray emission to evaluate the impact of AGN activity on the ISM gas. We employ X-ray data from the All Wavelength Extended Groth Strip International Survey (AEGIS) project (Davis et al. 2007) to obtain the X-ray surface brightness profiles of our samples. The AEGIS-X survey (Nandra et al. 2007) optimizes the balance between depth and sky area covering a sky region of 0.67 deg^2 in the energy range 0.5 – 7 keV. The survey region has been scanned at many wavelengths from radio to X-rays. The wide field of view, and the broad coverage in redshift along with multi-wavelength observations makes it a premier dataset for studying AGN co-evolution. We perform a stacking analysis of X-ray maps of AGN and normal galaxies from the AEGIS-X survey and compare their mean X-ray surface brightness profiles to investigate the effect of AGN on the ISM.

Our paper is organized as follows. In §2 we give a brief description of our datasets. In §3 we describe the methodology. We present our results in §4. We finally discuss our results and summarize our conclusions in §5 and §6. Throughout the paper we assume a spatially flat, Λ CDM cosmology: $\Omega_m = 0.28$, $\Omega_\Lambda = 0.72$, $\Omega_b = 0.04$, and $h = 0.71$.

2. DATA SETS

For the purpose of our analysis we use data from the AEGIS-X survey (Laird et al. 2009; L09 hereafter) and the DEEP2 Galaxy Redshift Survey (Davis et al. 2003; Newman et al. 2013). In this section we will provide a brief description of our datasets.

2.1. X-ray AGN sample

The AEGIS-X survey consists of 8 deep *Chandra* ACIS-I pointings, each with a total integration time of about 200 ks covering an area of 0.67 deg^2 . Details of data reduction are discussed in L09. The individual observations are merged into a single event file and images are constructed in four energy bands 0.5-7.0 keV (full), 0.5-2.0 keV (soft), 2.0-7.0 keV

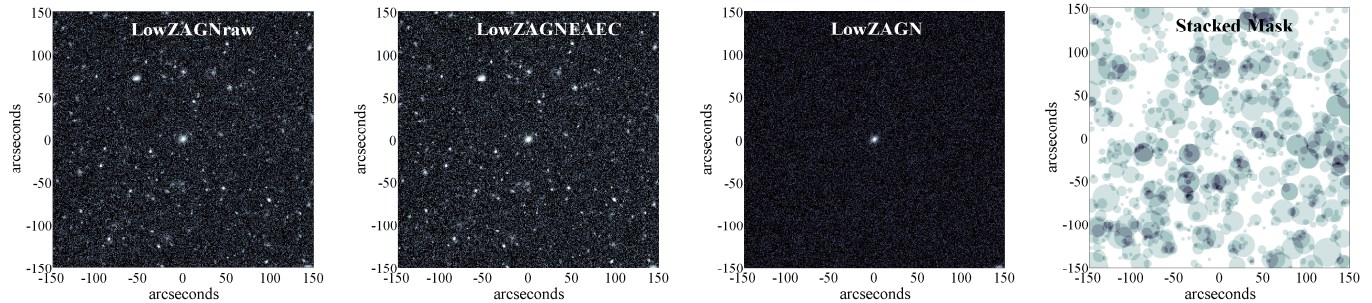


FIG. 2.— Methodology for constructing our stacked maps. All the maps are for the soft band corresponding to the L09 *Lowz* sample. The method is described in §3. The left-most panel shows the stacked map of the raw event files. This map is not corrected for exposure time or effective area. Also the point sources are not masked in this map. The middle-left panel shows the same map after correcting for exposure time and effective area. The point sources are still not masked in this map. We call this the EAEC map. We emphasize that these two maps are for illustrative purposes and we do not construct them in practice for our actual analyses. We correct the 8 EGS event files with the corresponding effective area-exposure time maps and conduct our analyses. See §3 for more discussion. The middle-right panel shows the exposure time effective area corrected map, where the point sources are masked using the method described in L09. The right-most panel shows the stacked mask map. Our final maps (shown in Fig. 3) are constructed by dividing the middle-right panel by the right-most panel.

(hard) and 4.0-7.0 keV (ultra-hard). The limiting flux in each of these bands is estimated to be 2.37×10^{-16} , 5.31×10^{-17} , 3.76×10^{-16} and $6.24 \times 10^{-16} \text{ erg s}^{-1} \text{ cm}^{-2}$, respectively (L09). We use the soft band for our analysis.

A point source catalog of the Extended Groth Strip (EGS) field has been provided in L09. The catalog consists of a total of 1325 band-merged sources with a Poisson probability limit of 4×10^{-6} . The source detection algorithm is described in Nandra et al. (2005). The basic technique is based on pre-detection with a low signal-to-noise threshold and follow-up aperture extraction of the photon counts to determine the detection significance of the source. The X-ray catalogs were matched to the DEEP2 optical photometry catalog (Coil et al. 2004) to account for positional offsets.

To select our AGN sample from the point source catalog of L09 we applied the following cuts to the dataset. We first applied a cut on the soft X-ray luminosities of our sources and selected objects with soft X-ray luminosities $\geq 10^{41} \text{ erg s}^{-1}$. The luminosity cut should retain only sources with X-ray emission due to AGN. We then applied a redshift cut to our sample ($0.3 \leq z \leq 1.3$) to be consistent with the bulk of the range covered by galaxies with secure redshifts from the DEEP2 Galaxy Redshift Survey.

Finally we restricted our analysis to the sources that have good quality spectroscopic redshift measurements from DEEP 2. For our AGN sources we have additional spectroscopic redshifts from MMT (Coil et al. 2009). This is required to construct a reliable control sample of galaxies for reasons described in §2.2. Out of the 1325 sources 477 of them have DEEP2 counterparts. 194 of them have redshift measurements. The high quality spectroscopic redshift criterion, and the subsequent redshift and luminosity cuts reduce our sample size to 96 AGN.

For our surface brightness analysis we construct two redshift subsamples which we will refer to as *Lowz* ($0.3 \leq z \leq 0.7$: 51 sources) and *Highz* ($0.7 \leq z \leq 1.3$: 45 sources). The redshift limit between the two samples was selected at the median of the distribution. In Fig. 1 we show the luminosity (left panel) and redshift (right panel) distributions of our X-ray AGN sources. In both panels, the distributions are normalized by the total number of objects in each subsample.

2.2. Galaxy Control Sample

It is well known that ISM properties should depend on both the stellar mass of a galaxy and its color (e.g., cold gas fractions and virial temperatures are related to these properties of a galaxy). Hence, if we want to identify impacts of AGN activity on galaxies, we must compare samples that are matched in stellar mass and color. Luminosity and color provide excellent proxies for stellar mass and color (e.g., Bell & de Jong 2001). We also expect X-ray properties to depend on redshift—since galaxy ages, luminosity distance, angular diameter distance, and surface brightness dimming will all evolve with redshift. We therefore construct a set of galaxies which matches the distribution of our AGN in color, luminosity, and redshift. We also note that the large scale environments of galaxies and AGN will affect the ISM emission significantly. Studies show that there is no statistically significant difference between the environments of AGN and of other galaxies that are matched in color and luminosity (e.g., Georgakakis et al. 2007; Montero-Dorta et al. 2009). Thus minimal effect due to differences in environment is ensured through the matched samples of galaxies and AGN. Hence, if AGN feedback has no short-term effects, the ISM emission from both our AGN and our control galaxy sample should be identical.

The galaxy control samples for the L09 objects were constructed using the method described in Cooper et al. (2009). The objects are matched to the AGN sample within the 3 dimensional parameter space of B band absolute magnitude, restframe $U - B$ color, and redshift. The initial control sample consisted of 5000 galaxies, of which 2982 galaxies are unique. Some of the galaxies are stacked multiple times to ensure matched distributions of all parameters (i.e., color, redshift and luminosity). For extracting the surface brightness profiles we divide the galaxy sample into two redshift subsamples, using the same cuts as for the AGN redshift subsamples. The redshift distribution of the comparison sample is shown as the solid lines in the right panel of Fig. 1.

3. METHODOLOGY

Our measurements depend on the source stacking technique. In Fig. 2 we summarize the main components of our data stacking methodology using the example of *Lowz* L09 sources. The event files, the exposure time maps and the effective area maps are provided in L09. We first divide our event files by the exposure time-effective area maps. We

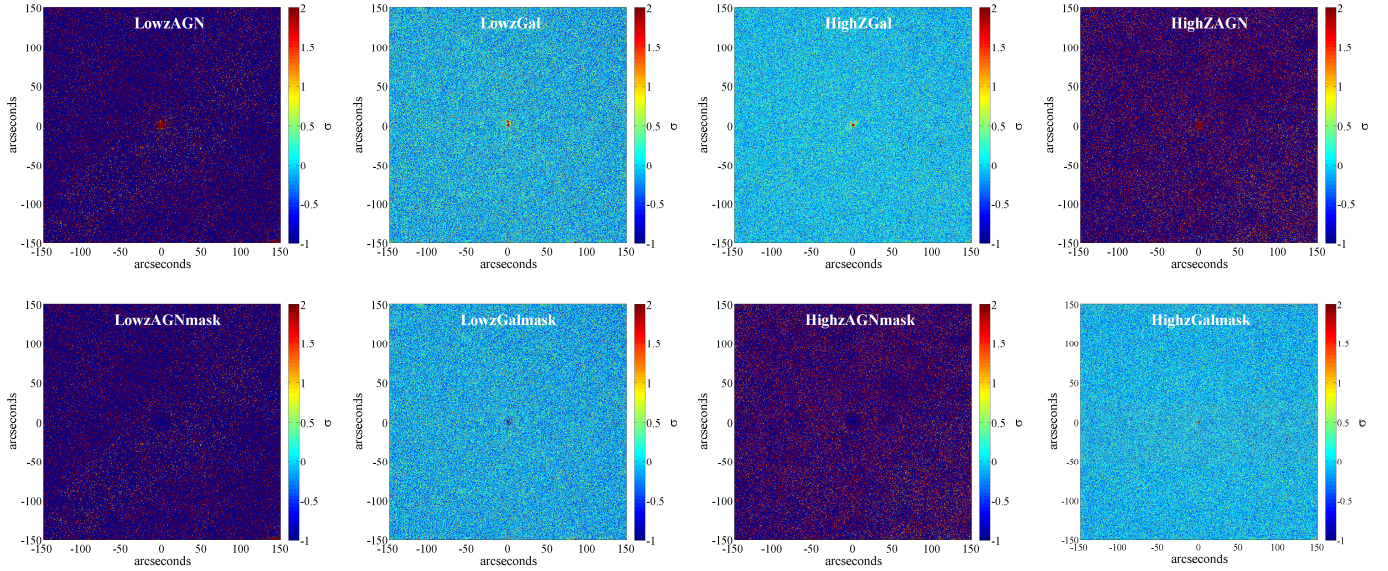


FIG. 3.— The stacked maps of galaxies and AGN. We subtract the background counts from each of these maps and divide by the background counts. Thus the maps represented here are essentially signal-to-noise (σ) maps. The top panel shows the maps where the central sources are unmasked. The bottom panels represent the same maps where the sources are masked. *Highz* and *Lowz* denote the redshift subsamples described in §2.1. The methodology for constructing these maps is shown in Fig. 2 and is described in §3.

call these effective area-exposure corrected (EAEC hereafter) maps. The gaps and singularities in the EAEC maps are corrected by assigning zero counts to those pixels where the EAEC maps have singularities (due to zero exposure and/or effective area). We then identify sources in the EAEC maps and select a 5×5 square arcminute region around each source and sum them to construct the stacked image.

Since we are interested in extended emission we mask the point sources in our stacked maps. We identify the point sources in each map from the point source catalog presented in L09. We calculate the point spread function (PSF) for each point source using the technique described in L09. The *getpsf* routine, provided by L09, is used to obtain the PSFs. We then mask the point sources using the ellipse corresponding to the 95% encircled energy radius (EER). We mask the region which encompasses a circular area with a radius 1.5 times that of the semi-major axis of the 95% encircled energy ellipse of a particular point source. This allows us to create a conservative mask for each point source.

We also construct a stacked mask map (shown in the right-most panel of Fig. 2). For our sources (galaxies and AGN) we adopt two methods. In one case the sources are not masked (shown in the top panel of Fig. 3) and in the other case we mask our sources (shown in the bottom panel of Fig. 3). It is important to note that a source in one map could be a potential contaminant point source (to be masked) in another map. The left-most panel of Fig. 2 shows the raw stacked map of the L09 *Lowz* AGN sources in the soft band. Note that we do not apply any exposure time or effective area correction for this map and the point sources are unmasked. The left-middle panel shows the same map but now corrected for exposure time and effective area. However the point sources are still unmasked in these maps. We emphasize that the maps presented in the left-most and middle-left panels of Fig. 2 are for illustrative purposes only and have not been used in our actual analyses. In the middle-right panel we present the stacked map where the point sources are masked (excluding the cen-

tral source). The right-most panel shows the stacked mask map. We divide the middle-right map by the right-most map to obtain the final maps shown in Fig. 3.

Extracting surface brightness profiles requires subtraction of the background counts. We calculate the background counts using the average counts from a region that is larger than ten times the area of the PSF. We also require the region for background extraction to be sufficiently far away from our sources. In our current analysis the background counts are extracted from the annular region between 50 arcseconds and 70 arcseconds from the sources. The background count has been calculated using the stacked masked maps of our galaxies and AGN. We verified that changing the area of the region for background extraction does not affect the estimated background provided it is sufficiently far from the sources. The background count in the soft band is estimated to be $1.66 \times 10^{-10} \text{ cm}^{-2} \text{ s}^{-1} \text{ pixel}^{-1}$. For a 200 ksec exposure and an effective area of 350 cm^2 the background count is ~ 0.012 per pixel.

To compare the surface brightness profiles of the AGN and galaxy maps we compute the spatial profiles of the mean photon counts of the two samples. We note that the total emission in the region is a combination of both diffuse emission in the ISM/ICM and the emission from the central nucleus. Since we are focused only on extended emission, we adopt a simple calibration to convert counts to flux. We assume that the average energy of each photon is equal to the average energy of the soft band (1.25 keV). This provides an order of magnitude estimate of the energy scales involved. The actual flux will depend on the spectrum and will be $\langle \text{flux} \rangle / (1.25 \text{ keV})$, which should be of order unity: an estimate on uncertainties in the flux calibration.

To separate the diffuse emission from the nuclear emission we construct a model PSF for our sources. We assume a Gaussian profile for the PSF, and from the *getpsf* routine we extract the 50% EER, 60% EER, 70% EER, 80% EER, 90% EER and 95% EER for each source. For our purpose we al-

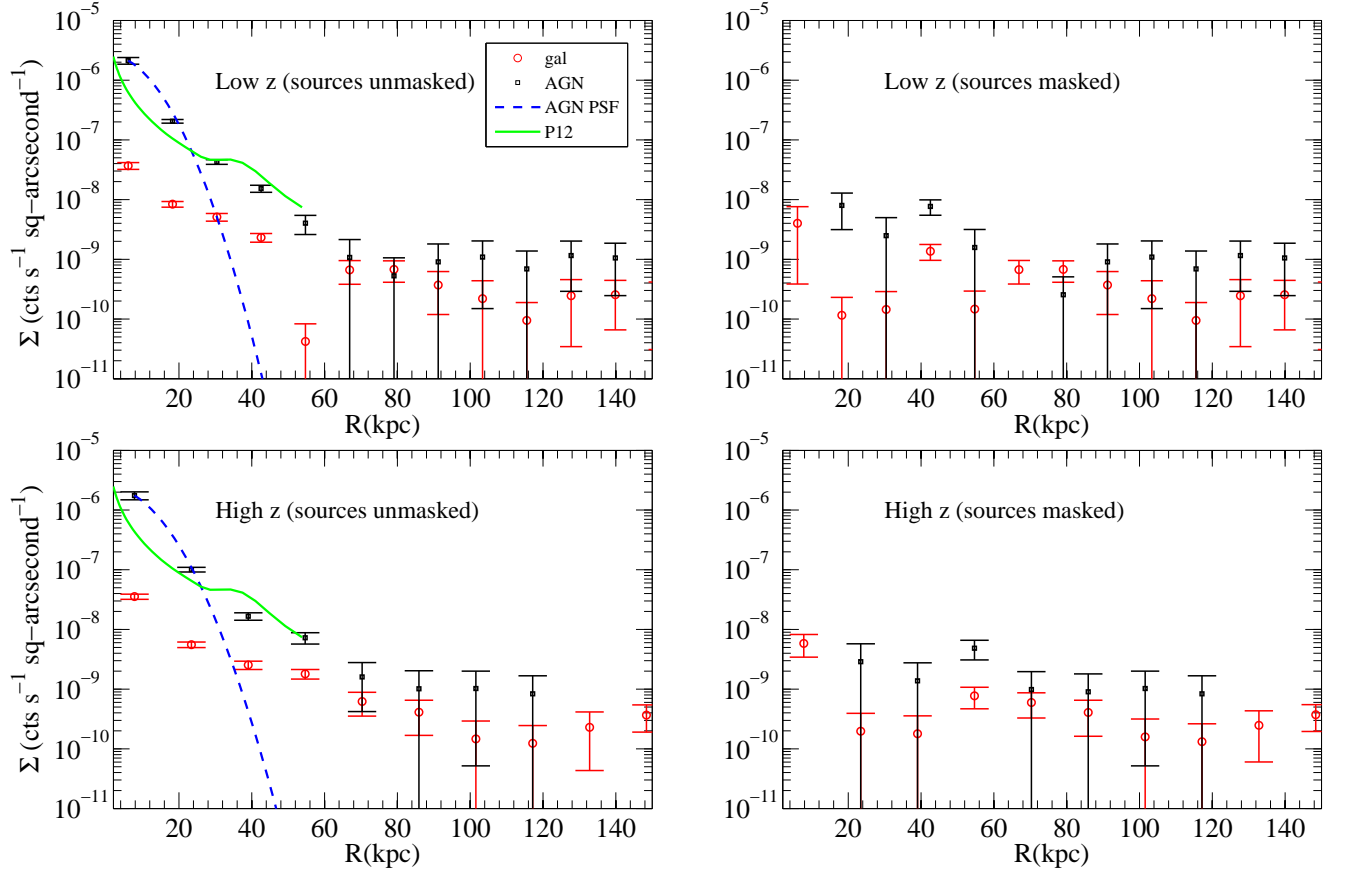


FIG. 4.— Surface Brightness Profiles of AGN and galaxies. The units are in $\text{cts s}^{-1} \text{sq-arcsecond}^{-1}$. In both panels black squares correspond to the AGN sample and red circles correspond to galaxies. The blue dashed line represents the average PSF model for our AGN sources and the green solid line is the theoretical profile from P12 with AGN feedback. The magnitude of the extended emission is in agreement with P12. The method for constructing the average PSF is discussed in §3. We clearly detect an extended emission beyond the PSF scale. The top and bottom panels represent the *Lowz* and *Highz* subsamples respectively. The left panel shows the AGN profiles where the central AGN/galaxy sources have not been masked (as discussed in §3 and shown in the top panels of Fig. 3). The right panel shows the profiles where the central sources have been masked (bottom panels of Fig. 3). See Fig. 5 and §4 for discussion on the weighted mean difference profiles.

ways consider the auxiliary circle (with a radius equal to the semi-major axis) corresponding to the PSF ellipse, which is a conservative estimate of the PSF. The EER correspond to the radii within which the total integrated flux will be the appropriate fraction (f) of the total flux. Thus the inverse of the integrated Gaussian function (which is the error function) will be equal to the EER scale for a fraction f . By inverting this equation we can extract the width of the Gaussian. Since for each source we have six values of the EER, we extract the width of the profile from all six values of the EER. We note that all six EER values return similar widths for the Gaussian profile. For each source we then identify the mean of these six values as the PSF width of that particular source. We then take the median width of all the sources as our average PSF profile. We normalize the PSF profile to the peak emission of our AGN surface brightness profile to do a fair comparison. The average PSF profiles are shown as blue dashed lines in Fig. 4.

4. RESULTS

We extract the surface brightness profiles from the average stacked maps (shown in Fig. 3). The X-ray profiles for the L09 and control samples are shown in Fig. 4. The units are in $\text{cts s}^{-1} \text{sq-arcsecond}^{-1}$. To obtain the profiles we estimate

the mean count (per pixel) and the standard error (standard deviation/ \sqrt{N} : N being the total number of pixels in each annulus) on the mean at each annulus. The top and the bottom panels represent the profiles for the *Lowz* and *Highz* samples respectively. The left panel shows the AGN profiles where the central sources have not been masked (as discussed in §3 and shown in the upper panels of Fig. 3). The right panel shows the profiles where the central sources have been masked (presented in the lower panels of Fig. 3).

To convert to physical scale we used the median redshift of the two samples. The median redshifts for the *Lowz* and *Highz* samples are 0.51 and 0.86 respectively. In the right panels (where the sources are masked) we find an excess in the AGN counts for both the samples within a scale of 40–60 kpc. There is a deficit in AGN counts at scales below 20 kpc (right panels of Fig. 4). The blue dashed lines in the left panels show the average PSF profiles (discussed in §3) for our *Lowz* and *Highz* AGN sources. We note that in both cases we detect significant emission ($\sim 1\text{--}4\sigma$) at scales between 40–60 kpc, well beyond the PSF scales. In §5.1 we discuss the possible systematic effects that may impact the final results in using the conversion from angular to physical scale at the median redshift and assuming a single PSF scale for all sources. The solid green line shows the theoretical profile with AGN

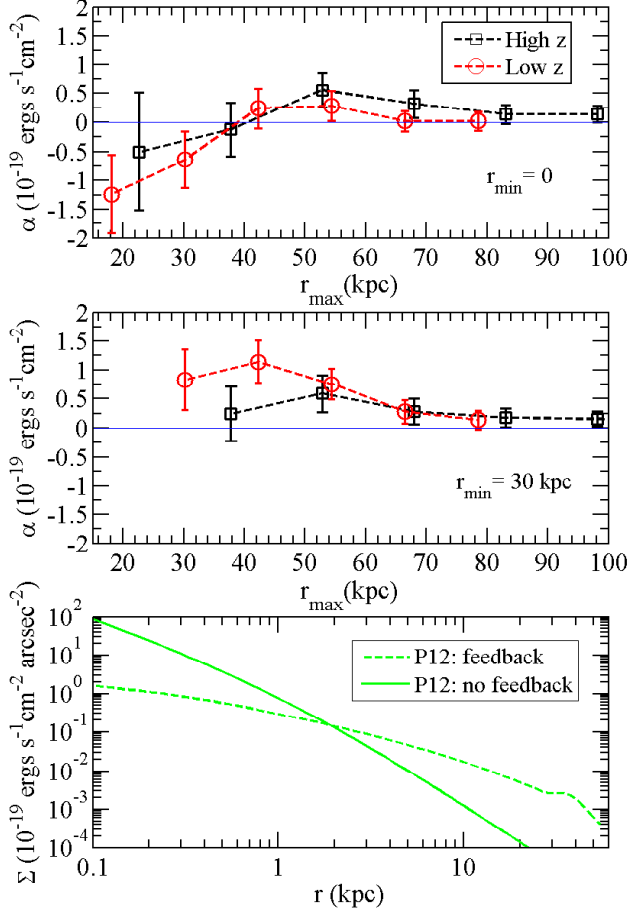


FIG. 5.— The weighted mean difference in the photon flux (quantified as α in Eq. 1) between the AGN and galaxy profiles as a function of spatial scale. For computing α we used the profiles in the right panels of Fig. 4. Positive (negative) numbers imply an excess (deficit) of X-ray flux in the AGN case. Black squares represent α for the *Highz* sample. The top and middle panels are for $r_{\text{min}} = 0$ and $r_{\text{min}} = 30 \text{ kpc}$. In the top panel we observe a slight excess (1.5σ) within a scale of 50 kpc. For the *Lowz* sample (red open circles) we observe a 1σ excess in photon flux when averaged over a scale of $\sim 50 \text{ kpc}$. We see a deficit (1.5σ) at a $r_{\text{max}} = 18 \text{ kpc}$. The solid blue line represents $\alpha = 0$. For $r_{\text{min}} = 30 \text{ kpc}$, we observe a 3σ excess in the *Lowz* profile. To compare with P12 we plot the theoretical ISM profiles for models with (green dashed) and without (green solid) feedback in the bottom panel. We note that our observed trend of excess and deficit is similar to the theoretical predictions by P12. Our analysis is limited by spatial resolution to make a one-to-one comparison with P12.

feedback from P12. The magnitude of our extended emission is in agreement with the theoretical predictions.

From clustering measurements and from studies of environments it has been shown that AGN observed in the EGS field tend to reside in more massive halos (e.g., Montero-Dorta et al. 2009; Coil et al. 2009). The typical host halo mass scale of these AGN is $\sim 10^{13} M_{\odot}$ (Coil et al. 2009). This would imply a somewhat more extended emission around them, as is seen in the present case. The effect will be similar for the galaxy control sample which has been matched in color and luminosity with the AGN host galaxies and thus having similar environments as AGN host galaxies (see discussion in §2.2).

To quantify the differences in the counts we compute the statistic α which is essentially the weighted mean difference of counts. For computing α we used the profiles in the right

panels of Fig. 4. α is defined as

$$\alpha = \frac{\sum_{r_{\text{min}}}^{r_{\text{max}}} \frac{(\text{count}_{\text{agn}} - \text{count}_{\text{gal}})}{\sigma_{\text{diff}}^2}}{\sum_{r_{\text{min}}}^{r_{\text{max}}} \frac{1}{\sigma_{\text{diff}}^2}}$$

$$\sigma_{\text{diff}} = \sqrt{\sigma_{\text{agn}}^2 + \sigma_{\text{gal}}^2}$$

$$\sigma_{\alpha}^2 = 1 / \sum_{r_{\text{min}}}^{r_{\text{max}}} \frac{1}{\sigma_{\text{diff}}^2}, \quad (1)$$

where $\text{count}_{\text{agn}}$ and $\text{count}_{\text{gal}}$ are the mean counts in each annulus for the AGN and the galaxy samples, σ_{agn} and σ_{gal} are the errors on mean counts in each annulus for the AGN and the galaxy samples, and r_{min} and r_{max} correspond to the range of annuli over which we are averaging. Hence, α is the inverse-variance-weighted mean of the difference in counts, averaging over the radius range r_{min} to r_{max} . The values and the 1σ errors on α are shown in Fig. 5. In each case r_{min} has been fixed to 0 (top panel of Fig. 5) and 30 kpc (middle panel of Fig. 5, beyond the PSF scale).

In Fig. 5 we present α (in flux units) as a function of r_{max} . Positive (negative) numbers imply an excess (deficit) of X-ray flux in the AGN case. We use two values of r_{min} to quantify the difference. Black squares represent the difference for the *Highz* sample. In the top panel ($r_{\text{min}} = 0$) we observe a 1σ excess in flux at $r_{\text{max}} = 50 \text{ kpc}$. For the *Lowz* sample (red open circles) at smaller scales ($< 20 \text{ kpc}$) we observe a slight deficit (1.5σ) in flux and a 1σ excess in flux at $r_{\text{max}} = 50 \text{ kpc}$. We emphasize that the excess/deficit in flux represents the average difference in flux between AGN and galaxies when averaged over a circular region with radius equal to r_{max} . In the middle panel ($r_{\text{min}} = 30 \text{ kpc}$) of Fig. 5 the significance of the excess for the *Lowz* sample enhances to $2 - 3\sigma$ depending on the physical scale.

In the bottom panel of Fig. 5 we show the theoretical ISM profiles derived using models with (dashed) and without (solid) feedback from P12. We find that the trend observed in Fig. 5 (top and middle panels) is similar to the theoretical predictions of P12. Although the significant excess seen in the middle panel of Fig. 5 implies that the profiles of the AGN and galaxies are not identical (at the 3σ level), this does not necessarily imply AGN feedback according to current models, since we can not probe whether there is the expected dip at smaller scales (see bottom panel of Fig. 5 and the discussions in §5.2). From the surface brightness profiles in Fig. 4 and the total flux in Fig. 5 we can estimate the total energy associated with the process. The total energy rate is given as $E (\text{ergs s}^{-1}) = 2\pi r d r \Sigma d_L^2$, where d_L is the luminosity distance. At scales of $40 - 60 \text{ kpc}$ at $z = .51$, this gives us an energy of $\sim 10^{36} - 10^{37} \text{ ergs s}^{-1}$.

5. DISCUSSION OF RESULTS

We now discuss some systematic effects that can potentially affect our results and then evaluate our findings in light of theoretical models.

5.1. Systematic Effects

As discussed above, we interpret the surface brightness profile to be the mean profile at the median redshift. We also adopt the median PSF as the average PSF of our sources. This interpretation is slightly problematic when we convert from angular scale to physical scale since there will be mixing of scales due to the variation in the angular diameter distance

and the variation in source PSFs. To examine the contamination from this effect we perform the following test. We compute the physical PSF scales for each source (both galaxy and AGN) with the corresponding redshifts and angular PSF scales. We find that the PSFs (discussed in §3) of most of our galaxy sources are well within 20 kpc at all redshifts with a few exceptions. For our AGN sources roughly 60% of PSFs are between 5–15 kpc and the remaining 40% are between 15–30 kpc. About 10% of our AGN sources have PSFs between 25–30 kpc.

We recomputed the weighted mean difference profiles after removing sources with larger PSFs. We find that the results (excess/deficit) do not show any significant change (except for slightly enhancing the errors in α at scales beyond 50 kpc) on excluding these large PSF sources. None of our AGN or galaxy sources have PSFs beyond 30 kpc. We find significant emission at scales above 30 kpc for both our AGN and galaxy sources and thus we are confident that the PSF contamination at these scales is minimal. This is also evident in the right panels of Fig. 4 where we still detect emission after masking the central sources with a very conservative mask. We do not detect emission at these scales from the hard or the ultra-hard bands.

To see if our results depend on the choice of our masking radius, we perform the following test. We restacked our maps using different values of the masking radii. Our fiducial maps have masking radii of 1.5 times the 95%EER. We repeated our analyses with mask sizes of 1.0 and 3.0 times the 95% EER. We find that our results do not depend on the choice of our mask size and results shown in Fig. 4 are statistically identical in each case. Although for more conservative masks the flux differences (Fig. 5) become increasingly insignificant. The results are similar to our fiducial mask sizes when we use a masking radius of 1.0 times the 95%EER.

To check if the excess seen in the right panels of Fig. 4 depends on our choice of binning we obtained several surface brightness profiles with smaller and larger spatial bin size than our fiducial binning. We find that binning has a small impact on the surface brightness profiles presented in the right panel of Fig. 4. Thus the scale at which we see this excess, can shift due to a different binsize. We emphasize that the weighted-mean-difference profiles (α in Eq. 1, shown in Fig. 5) recover our best estimate of the true comparison between AGN and galaxy photon distributions, and we interpret our results based on that.

5.2. Comparison with Theory

As discussed before, models of AGN feedback suggest that there should be a relationship between the outflows/energy from an AGN and the density and temperature distribution of gas in galaxies and clusters. However the magnitude and the scale of influence remain mostly uncertain. For example, studies suggest that the scale of influence of AGN feedback (where observable signatures are prominent) can vary from a few tens of kpc (e.g., P12) to a few hundred kpc (e.g., Chatterjee et al. 2008) to a few Mpc (e.g., Scannapieco et al. 2008) depending on the nature of the observable.

Based on simulations of an isolated elliptical galaxy (with a B -band luminosity of $L_B = 5 \times 10^{10} L_{B\odot}$) P12 found that the X-ray surface brightness profiles in galaxies are significantly different if the effects of feedback from an AGN are included. Differences in the surface brightness profile are evident even at radii beyond 50 kpc (bottom panel of Fig. 5). We note that the scale of influence where features in the surface

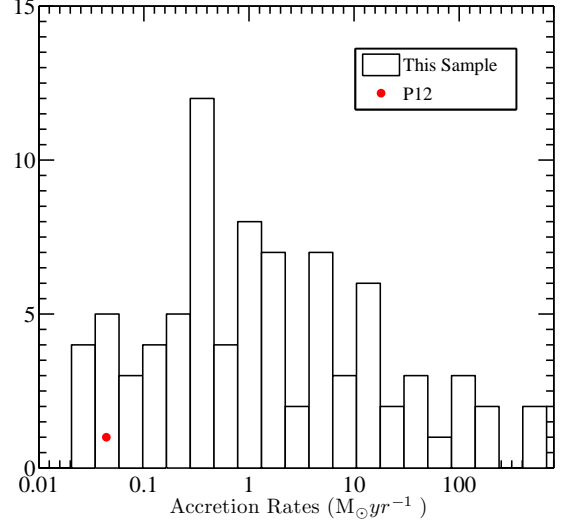


FIG. 6.— Distribution of approximate accretion rates of our AGN sample. The red data point represents the typical accretion rate of the black hole in the model galaxy of P12. See §5.2 for the method of computing accretion rates.

brightness profiles due to the nuclear outburst can be visible, is well within the PSF scales of our AGN sources. Without decomposing the observed emission into PSF-like and extended components, we cannot distinguish models based on features in the surface brightness profile at small radius. However large scale differences (~ 50 kpc) due to AGN feedback are likely to show up in the X-ray profiles. We search for such differences in the surface brightness profile.

Physically, feedback from AGN is likely to disrupt the ISM/ICM gas and transport it to a larger length scale from the center of the galaxy/cluster. This appears as bumps and cavities at larger (far from the black hole) and smaller (closer to the black hole) length scales in the X-ray surface brightness profiles. The scales of deficit and excess are a few kpc, and 10 – 50 kpc respectively for the model galaxy presented in P12 (Fig. 5 bottom panel). We find that the average B -band luminosity of our AGN host galaxies is $L_B = 1.45 \times 10^{10} L_{B\odot}$, in rough agreement with the model galaxy presented in P12. The data points at 46 kpc (Fig. 4 top right-panel) and 62 kpc (Fig. 4 bottom-right panel) show excess flux for the AGN hosts compared to the control sample but at other scales we do not detect any significant difference.

To further quantify this effect, we extracted the weighted-mean-difference profile (α in Eq. 1) in Fig. 5. We observe a deficit at scales below 20 kpc and an excess at scales around 40 – 60 kpc (top panel of Fig. 5). The trend of the excess ($\sim 1\sigma$) and deficit ($\sim 1.5\sigma$) observed in the weighted-mean-difference profiles is qualitatively similar to the theoretical predictions by P12. We find that for $r_{\min} = 30$ kpc, we detect a significant excess (3σ) in the *Lowz* AGN profile (middle panel of Fig. 5). This is in accordance with model predictions, but an accompanying deficit at small scales is required to strongly confirm the theory. We thus restrict ourselves from claiming that our results strongly support the paradigm presented in P12.

We clarify that the lack of a major difference between AGN and control samples (as predicted in P12), does not exclude the possibility that weak (below our noise level) differences do exist between AGN and galaxies and are undetected in our

analysis. We also note that a lack of difference between the AGN and control sample does not necessarily mean that AGN feedback has no effect. It is likely that the AGN that are visible in the X-ray are essentially just a random subset of all galaxies: those that happen to be accreting strongly enough to be detected *now*; but the duty cycle is short. Thus all of the objects in the control sample may have had AGN feedback recently too, but just happen to be currently “turned off”, and hence have a similar net profile. We discuss the possibility of extending this work with alternative AGN samples in §5.3.

Apart from the spatial scale of feedback the magnitude of feedback is an important quantity that remains uncertain in the literature. Theoretical models mostly assume feedback energy to be a fixed fraction of the accreted mass energy of the black hole, allowing more feedback from more luminous AGN (e.g., Di Matteo et al. 2005). We thus compare the approximate accretion rates of our AGN samples with that of P12. The accretion rates are compiled in the following way. The bolometric luminosities of our AGN sample were obtained from the X-ray luminosities using the bolometric corrections of Marconi et al. (2004). We then assume $\eta = 0.1$, a canonical efficiency for thin disk accretion (Shakura & Sunyaev 1973) and compute the approximate accretion rates of the black holes corresponding to our AGN sample. The distribution of accretion rates is shown in Fig. 6. The red data point corresponds to the accretion rate of the black hole in the model galaxy of P12.

The accretion rates of our sample are much higher than the typical accretion of the black hole in the model galaxy of P12. This implies that in the paradigm of “accretion rate dependent feedback” our AGN sample should have more feedback than the typical black hole of P12. This assumption is true if the estimated rates represent sustained feedback—*episodic* feedback, which is high at the moment we detect the AGN, could reconcile our higher feedback rates with the model of P12. From Fig. 5 we obtain a flux difference of $\sim 10^{-19}$ ergs s $^{-1}$ cm $^{-2}$ which is similar to the flux scales derived in P12 (bottom panel of Fig. 5).

5.3. Future Work

We note that our central sources were masked using a conservative mask (discussed in §3 and shown in the bottom panel of Fig. 3). The PSF broadening (~ 10 kpc scale) is entirely an instrumental effect and has no connection with the actual physical scale of AGN nuclear emission, which is limited to a few parsecs. Thus any difference in the surface brightness profile that appears at scales beyond a few parsec to a few tens of kpc will be suppressed due to the PSF contamination and the subsequent masking. Hence a sample of black holes that have comparable accretion rates to that of our X-ray AGN, but are under-luminous in X-rays will be an ideal sample for studying AGN/ISM interaction at scales of a few kpc. Confusion due to the nuclear emission will be limited in this case, making it easier to extract any extended emission. However this would be true if feedback is correlated to accretion rates only, which is assumed in many theoretical models. We propose to undertake these studies in a future paper.

The theoretical paradigm of “accretion rate dependent feedback” could be examined by comparing the X-ray surface brightness profiles of highly accreting black holes—e.g., quasars, for which the feedback energy is expected to be higher if we assume the feedback energy to be directly proportional to the bolometric luminosity/accretion rates of the AGN—to that of normal galaxies with identical optical prop-

erties to quasar hosts. Since inference about the optical properties of the host galaxies of quasars is difficult, the best sample with which to conduct this measurement might be a population of obscured quasars.

In addition, quasars may grow most in the obscured phase and hence would have the highest amount of feedback (Hopkins et al. 2008). If this paradigm is correct we would expect to see the maximum effect of feedback on X-ray surface brightness profiles around obscured quasars. However the success of this study will depend on the time scale of feedback. Feedback needs to be effective within a time scale of 10 Myrs (the typical lifetime of a luminous quasar). Some theoretical models suggest that about 20–30% of the quasar population undergo a rapid blowout phase (e.g., Hopkins et al. 2008). Thus a promising avenue will be to apply our analysis to study the effect of obscured quasars on the diffuse ISM.

6. SUMMARY

In this work, we perform a stacking analysis of X-ray selected AGN in the AEGIS field in the redshift range 0.3–1.3 and compare their average surface brightness profile to the average surface brightness profile of galaxies in the same field. Our AGN and galaxies are matched in optical properties and redshift distributions. We detect ISM emission at a scale of 40–60 kpc in both accreting and non-accreting galaxies, and demonstrate that any differences in surface brightness profiles due to X-ray visible AGN cannot be large. We divide our main sample into two redshift subsamples, *Lowz* ($0.3 \leq z \leq 0.7$) and *Highz* ($0.7 \leq z \leq 1.3$), and show that there exists differences between the X-ray surface brightness profiles of AGN and galaxies.

To quantify the differences, we extract the weighted-mean-difference profile (α in Eq. 1) from the surface brightness profiles. From theoretical modeling P12 finds deficit and excess in the surface brightness profiles for the case with AGN feedback, compared to the no feedback case at scales of few kpc, and 10 – 50 kpc respectively. The trend of the excess (40–60 kpc $\sim 1\sigma$) and deficit (< 20 kpc $\sim 1.5\sigma$) observed in the weighted-mean-difference profiles is qualitatively similar to the theoretical predictions by P12 but at a lower significance. However if we exclude the PSF scales (~ 30 kpc) of majority of our AGN sources, we do detect significant (3σ) excess in the AGN profile which is indicative of AGN feedback. Although the results seem promising we emphasize that we need to quantify both the excess and deficit to conclusively support the theoretical paradigm.

The observed lack of major difference (similar to P12) might be interpreted in the following ways: 1) AGN feedback has only a weak effect on the diffuse ISM gas (i.e. below the noise level of our detection) or 2) AGN that are visible in the X-rays are a random subset of all galaxies that are accreting strongly enough for detection but that have a short duty cycle. Under the latter interpretation, every galaxy in the control sample went through a similar feedback phase and thus we obtain identical X-ray profiles. Since the PSF contamination is higher for the X-ray bright sources, we propose that a sample of black holes that have comparable accretion rates to that of our X-ray AGN, but that are under-luminous in X-rays will be an ideal sample for studying the effect of feedback on the diffuse ISM gas. We also suggest that obscured quasars might have more effect on X-ray surface brightness profiles if the amount of feedback energy is directly proportional to the accretion rate of the black hole, as assumed in several theoretical models.

ACKNOWLEDGMENTS

SC would like to thank Nico Cappelluti for some discussions on background counts in our maps and Silvia Pellegrini for providing the theoretical data points from Pellegrini et al. SC thanks Daisuke Nagai for several useful discussions and acknowledges computational resources and support from YCAA. SC and JAN were partially supported by NSF grant AST-0806732 at the University of Pittsburgh. SC and ADM

were partially supported by the National Science Foundation through grant number 1211112, and by the National Aeronautics Space Administration (NASA) through ADAP award NNX12AE38G and Chandra Award Number AR0-11018C issued by the Chandra X-ray Observatory Center, which is operated by the Smithsonian Astrophysical Observatory for and on behalf of NASA under contract NAS8-03060. ALC acknowledges support from NSF CAREER award AST-1055081.

REFERENCES

- Arnaud, M., & Evrard, A. E. 1999, *MNRAS*, 305, 631
- Battaglia, N., Bond, J. R., Pfrommer, C., Sievers, J. L., & Sijacki, D. 2010, *ApJ*, 725, 91
- Bell, E. F., & de Jong, R. S. 2001, *ApJ*, 550, 212
- Bhattacharya, S., Di Matteo, T., & Kosowsky, A. 2008, *MNRAS*, 389, 34
- Birzan, L., Rafferty, D. A., McNamara, B. R., Wise, M. W., & Nulsen, P. E. J. 2004, *ApJ*, 607, 800
- Booth, C. M., & Schaye, J. 2009, *MNRAS*, 398, 53
- Cattaneo, A., Dekel, A., Devriendt, J., Guiderdoni, B., & Blaizot, J. 2006, *MNRAS*, 370, 1651
- Chatterjee, S., Di Matteo, T., Kosowsky, A., & Pelupessy, I. 2008, *MNRAS*, 390, 535
- Chatterjee, S., Ho, S., Newman, J. A., & Kosowsky, A. 2010, *ApJ*, 720, 299
- Chatterjee, S., & Kosowsky, A. 2007, *ApJ*, 661, L113
- Choi, E., Naab, T., Ostriker, J. P., Johansson, P. H., & Moster, B. P. 2013, *ArXiv e-prints*
- Choi, E., Ostriker, J. P., Naab, T., & Johansson, P. H. 2012, *ApJ*, 754, 125
- Ciotti, L., & Ostriker, J. P. 2001, *ApJ*, 551, 131
- . 2007, *ApJ*, 665, 1038
- Coil, A. L., Newman, J. A., Kaiser, N., Davis, M., Ma, C.-P., Kocevski, D. D., & Koo, D. C. 2004, *ApJ*, 617, 765
- Coil, A. L., et al. 2009, *ApJ*, 701, 1484
- Cooper, M. C., Newman, J. A., & Yan, R. 2009, *ApJ*, 704, 687
- Croton, D. J., et al. 2006, *MNRAS*, 365, 11
- Davis, M., et al. 2003, 4834, 161
- . 2007, *ApJ*, 660, L1
- Di Matteo, T., Springel, V., & Hernquist, L. 2005, *Nature*, 433, 604
- Dong, R., Rasmussen, J., & Mulchaey, J. S. 2010, *ApJ*, 712, 883
- Dunn, R. J. H., & Fabian, A. C. 2006, *MNRAS*, 373, 959
- Gaspari, M., Brighenti, F., D’Ercole, A., & Melioli, C. 2011, *MNRAS*, 415, 1549
- Gaspari, M., Brighenti, F., & Temi, P. 2012, *MNRAS*, 424, 190
- Gebhardt, K., et al. 2000, *ApJ*, 539, L13
- Georgakakis, A., et al. 2007, *ApJ*, 660, L15
- Giodini, S., et al. 2010, *ApJ*, 714, 218
- Gitti, M., Brighenti, F., & McNamara, B. R. 2012, *Advances in Astronomy*, 2012
- Hopkins, P. F., Hernquist, L., Cox, T. J., & Kereš, D. 2008, *ApJS*, 175, 356
- Hopkins, P. F., Robertson, B., Krause, E., Hernquist, L., & Cox, T. J. 2006, *ApJ*, 652, 107
- Johansson, P. H., Naab, T., & Burkert, A. 2008, *Astronomische Nachrichten*, 329, 956
- Johnson, R., Ponman, T. J., & Finoguenov, A. 2009, *MNRAS*, 395, 1287
- Kauffmann, G., & Haehnelt, M. 2000, *MNRAS*, 311, 576
- Laird, E. S., et al. 2009, *ApJS*, 180, 102
- Lapi, A., Shankar, F., Mao, J., Granato, G. L., Silva, L., De Zotti, G., & Danese, L. 2006, *ApJ*, 650, 42
- Marconi, A., Risaliti, G., Gilli, R., Hunt, L. K., Maiolino, R., & Salvati, M. 2004, *MNRAS*, 351, 169
- McNamara, B. R., & Nulsen, P. E. J. 2007, *ARA&A*, 45, 117
- Merritt, D., & Ferrarese, L. 2001, *ApJ*, 547, 140
- Montero-Dorta, A. D., et al. 2009, *MNRAS*, 392, 125
- Nandra, K., et al. 2005, *MNRAS*, 356, 568
- . 2007, *ApJ*, 660, L11
- Nath, B. B., & Roychowdhury, S. 2002, *MNRAS*, 333, 145
- Newman, J. A., et al. 2013, *ApJS*, 208, 5
- Novak, G. S., Ostriker, J. P., & Ciotti, L. 2011, *ApJ*, 737, 26
- Nulsen, P. E. J., Hambrick, D. C., McNamara, B. R., Rafferty, D., Birzan, L., Wise, M. W., & David, L. P. 2005, *ApJ*, 625, L9
- O’Sullivan, E., Giacintucci, S., David, L. P., Vrilek, J. M., & Raychaudhury, S. 2010, *MNRAS*, 407, 321
- Pellegrini, S., Ciotti, L., & Ostriker, J. P. 2012, *ApJ*, 744, 21
- Peterson, J. R., & Fabian, A. C. 2006, *Phys. Rep.*, 427, 1
- Puchwein, E., Springel, V., Sijacki, D., & Dolag, K. 2010, *MNRAS*, 406, 936
- Randall, S. W., et al. 2011, *ApJ*, 726, 86
- Scannapieco, E., & Oh, S. P. 2004, *ApJ*, 608, 62
- Scannapieco, E., Thacker, R. J., & Couchman, H. M. P. 2008, *ApJ*, 678, 674
- Schawinski, K., Thomas, D., Sarzi, M., Maraston, C., Kaviraj, S., Joo, S.-J., Yi, S. K., & Silk, J. 2007, *MNRAS*, 382, 1415
- Shakura, N. I., & Sunyaev, R. A. 1973, *A&A*, 24, 337
- Shankar, F., Salucci, P., Granato, G. L., De Zotti, G., & Danese, L. 2004, *MNRAS*, 354, 1020
- Sijacki, D., Springel, V., Di Matteo, T., & Hernquist, L. 2007, *MNRAS*, 380, 877
- Sunyaev, R. A., & Zeldovich, Y. B. 1972, *Comments on Astrophysics and Space Physics*, 4, 173
- Teyssier, R., Moore, B., Martizzi, D., Dubois, Y., & Mayer, L. 2011, *MNRAS*, 418
- Thacker, R. J., Scannapieco, E., Couchman, H. M. P., & Richardson, M. 2009, *ApJ*, 693, 552
- Tremaine, S., et al. 2002, *ApJ*, 574, 740
- Wyithe, J. S. B., & Loeb, A. 2003, *ApJ*, 595, 614